Dynamics of Photoinduced Electron Transfer in a Molecular Donor−Acceptor Quartet

Lin X. Chen,*,† Shengqiang Xiao,‡ and Luping Yu*,‡

Chemistry Division, Argonne National Laboratory, 9700 South Cass Avenue, Argonne, Illinois 60439, and Department of Chemistry and James Franck Institute, The University of Chicago, 5735 South Ellis Avenue, Chicago, Illinois 60637

Received: December 25, 2005; In Final Form: April 3, 2006

The electronic structures and dynamics of photoinduced charge separation and recombination in a new donor/acceptor quartet molecule with bis-oligothiophene (**BOTH**) and bis-perylenediimide (**BPDI**) blocks attached to a benzene ring were described. Detailed transient spectroscopic studies were carried out on this compound and reference compounds at isolated molecular levels in solution. Two different dynamics of charge separation and recombination associated with two types of donor/acceptor pair conformations in solution were observed. These results were discussed based on Marcus theory and ascribed to both through-bond and through-space electron-transfer processes associated with two different orientations of the acceptors relative to the donor group. This molecular system exhibits a more efficient charge separation than charge recombination processes in both polar and nonpolar organic solvents, indicating that the material is an interesting candidate for photovoltaic studies in solid state.

Introduction

Photoinduced electron transfer through a series of organic chromophores resulting in charge separation across the cell membrane is a key primary process in natural photosynthesis, the main source for solar energy conversion in nature.[1] Extensive studies have been carried out to understand dynamic, structural, environmental, and energetic components that determine reaction rates and efficiencies in photoinduced electron-transfer processes.[2−8] Inspired by the highly efficient charge separation reaction in natural photosynthesis, many antenna-donor−acceptor systems consisting of covalently linked discrete organic chromophores in well-defined orientations have been rationally synthesized and their reaction dynamics for photoinduced electron transfer have been investigated, aiming at producing materials with efficient and controllable photoinduced charge separation.[9−15] These studies laid foundations at molecular levels for design and assembly principles for organic donor/acceptor building blocks in potential photovoltaic applications.

Most of the organic photovoltaic materials studied so far, such as CuPc/C_{60} (Pc. phthalocyanine)[16−23] and diblock copolymers,[24−27] are noncovalent microscopic mixtures of multiple organic compounds that act as either electron donors or acceptors. When excitons are generated in these materials by light illumination, they must be able to diffuse to the boundaries between the microscopic donor/acceptor domains to dissociate into opposite charge carriers, which then need to be collected by respective electrodes to generate electricity. The exiton diffusion lengths in organic semiconductor materials are on the order of multiple nanometer scales,[20,22,28,29] much shorter than the microscopic donor/acceptor domain sizes in most of the current organic or hybrid solar cells. Consequently, the quantum yield of charge separation in these materials is low, which has been considered the bottleneck of the overall efficiency of organic photovoltaic solar cells.[30] Approaches have been proposed and implemented in growing interpenetrating microscopic donor and acceptor columns to enhance the yield of dissociation of excitons to charge carriers.[31,32]

Our approach in developing organic photovoltaic materials intends to break the bottleneck for the exciton dissociation in organic photovoltaic materials by covalently linking the donor and acceptor blocks as shown in a new donor−acceptor quartet molecular system in Scheme 1 of the Supporting Information. Meanwhile, the molecule is designed to be capable of self-assembly through $\pi-\pi$ stacking. Our rationale is to create donor and acceptor domains with sizes of a couple of nanometers to be compatible with the exciton diffusion length, allowing the excitons to dissociate at the molecular level. On one hand, the covalent linkage between the donor and acceptor blocks converts the photoinduced charge separation into an intramolecular process that removes the bottleneck of the exciton diffusion/dissociation. On the other hand, the sizes, shapes, and chemical properties of the donor−acceptor blocks can be chemically tuned, so the blocks that are alike can self-assemble through $\pi-\pi$ stacking[33] into channels in solid-state film for efficient transport of charge carriers and reduction of wasteful charge recombination. Compared with previous approaches of mixing donor and acceptor blocks with micrometer scale domains, this approach with better defined chemical structures allows accurate structural/functional characterization at different levels from single molecules to self-assembled films as well as prototype devices.

It is well recognized that an efficient organic photovoltaic device requires more than efficient photoinduced charge separation at the single molecular level, and the kinetics of fundamental physical processes in solid films can be drastically different from those in solution. As an initial study, a donor/acceptor quartet molecule with bis-oligothiophene (**BOTH**) and bis-perylenediimide (**BPDI**) blocks attached to a benzene ring (Figure 1) is synthesized and its electronic structures and photoinduced charge separation−recombination dynamics are characterized in dilute

* To whom correspondence should be addressed. E-mail: lchen@anl.gov; lupingyu@uchicago.edu.
† Argonne National Laboratory.
‡ The University of Chicago.

10.1021/jp057508e CCC: $33.50
Published on Web 05/25/2006

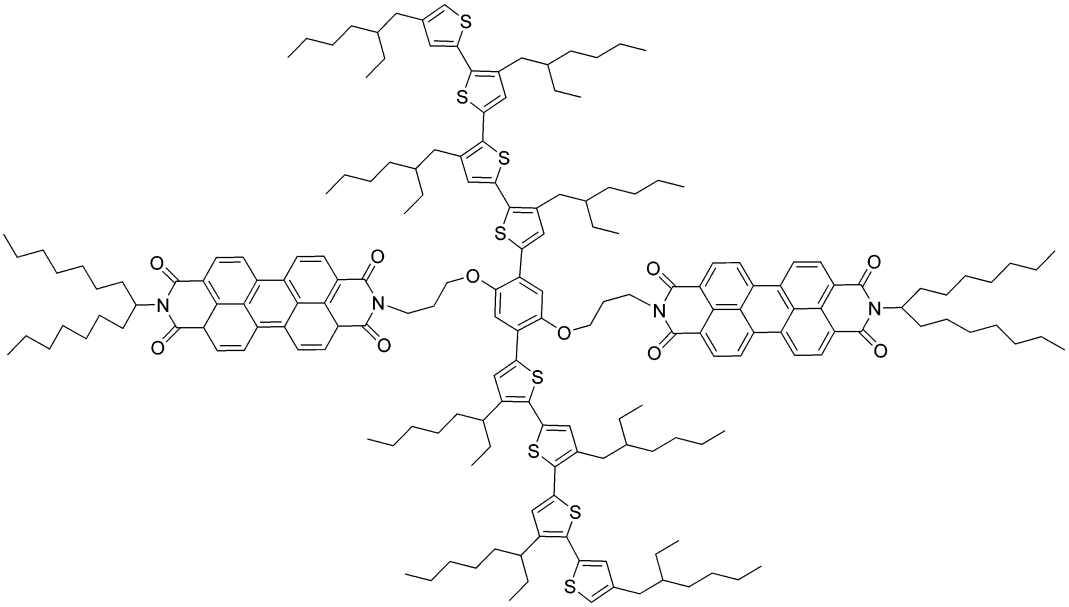

Figure 1. Structure of the **BOTH**−**BPDI** quartet molecule.

solution. More efficient charge separation (CS) than charge recombination (CR) processes have been observed in both polar and nonpolar organic solvents. The results also strongly suggest that two different dynamics of CS and CR are associated with at least two types of donor/acceptor pair conformations in solution, representing through-bond and through-space electron-transfer processes. This study provides initial screening for its potential organic photovoltaic applications. Extensive studies on the self-assembled films of this material as well as its photovoltaic characteristics are in process and will be published separately.

Experimental Methods

Synthesis. The structure of the quartet molecule (**BOTH**−**BPDI**) shown in Figure 1 was synthesized in three steps as described in the Supporting Information. Detailed characterizations confirmed the molecular structure as shown in Scheme 1 of the Supporting Information.

Femtosecond Transient Absorption Spectroscopy. Ultrafast transient absorption (TA) spectral and kinetics were measured by an amplified Ti:sapphire laser system with an optical parametric amplifier (OPA) as described elsewhere.[34] Excitation laser pulses were derived from either the second harmonic of the Ti:sapphire regenerative amplifier at 403 nm or the output of the OPA at 527 nm. White light continuum probe pulses were generated by focusing a few microjoules of the Ti:sapphire amplifier output onto a sapphire disk. The resulting probe beam was split into the reference and the measuring beams. The white light probe beam and the 300-nJ (∼100 nJ with OPA output) pump beam were focused to a 0.3-mm diameter spot at the sample with a nearly collinear geometry. The optical density of the sample was kept below 0.4 at 403 nm, and the sample cuvette was 2-mm thick. The pump and probe pulses were about 90-fs fwhm (full width at half-maximum), and the instrumental response function was 180-fs fwhm.

Stock solutions of the quartet and reference compounds were freshly made and were checked by a UV−vis spectrometer during laser experiments for possible photodegradation. The solutions were purged with a steady flow of nitrogen gas bubbling through a syringe. The sample cuvette was sealed by a septum during the experiments. All measurements were carried out at room temperature at 293 K.

Steady-state Absorption and Fluorescence Spectra. UV−vis measurements were made with a Shimadzu UV-2401PC recording spectrophotometer. Fluorescence data were obtained with a Shimadzu RF- 5301PC spectrofluorophotometer.

Electrochemistry. Cyclic voltammetry was performed on a CV-50W Voltammetric Analyzer (Bioanalytical Systems Inc.) in a conventional three-compartment cell in a solution of methylene chloride (0.1 M Bu4NPF6 as supporting electrolyte) at a scan rate of 100 mV/s. Solvent was dried and deoxygenated before use. A Pt wire was used as working electrode. Another Pt wire was used as the counter electrode, and a Ag/AgCl electrode was used as the reference electrode, calibrated against the oxidation of ferrocene. All oxidation and reduction potential values were reported against this Fc/Fc+ oxidation couple.

Results

Steady-state Absorption and Emission Spectra. Steady-state absorption spectra of the quartet molecule along with those of the reference compounds perylene diimide (**PDI**) and bis-oligothiophene (**BOTH**) in chloroform at room temperature are depicted in Figure 2. The reference compound **PDI** shows characteristic absorption peaks at 526, 490, and 459 nm which are denoted to its (0,0), (0,1), and (0,2) bands, respectively. These features remain almost identical in the quartet molecule, where the (0,0) band originating from the **BPDI** blocks shifts to red only by 2 nm relative to that of the reference compound **PDI**. The reference compound **BOTH** has a broad absorption band with a maximum at 431 nm, corresponding to the $\pi-\pi^*$ transition of the conjugated oligothiophene backbone in solution. On one hand, the absorption maximum of **BOTH** is near that of sexithiophene in the same solvent[35] suggesting that the π-conjugation is extended beyond a single quarterthiophene block through the coupling by the benzene ring. On the other hand, the energy corresponding to the absorption maximum of **BOTH** is still higher than that of an octithiophene segment,[35] indicating an attenuated π-conjugation in **BOTH** compared with that in an uninterrupted octithiophene, similar to those oligophenylenevinylene (OPV) derivatives with attenuated π-conjugation due to the insertion of different aromatic groups in the π-conjugated backbone.[36] The absorption spectrum of the quartet molecule can be reconstructed by a summation from those of the reference compounds **PDI** and **BOTH** with a 2:1 ratio. This

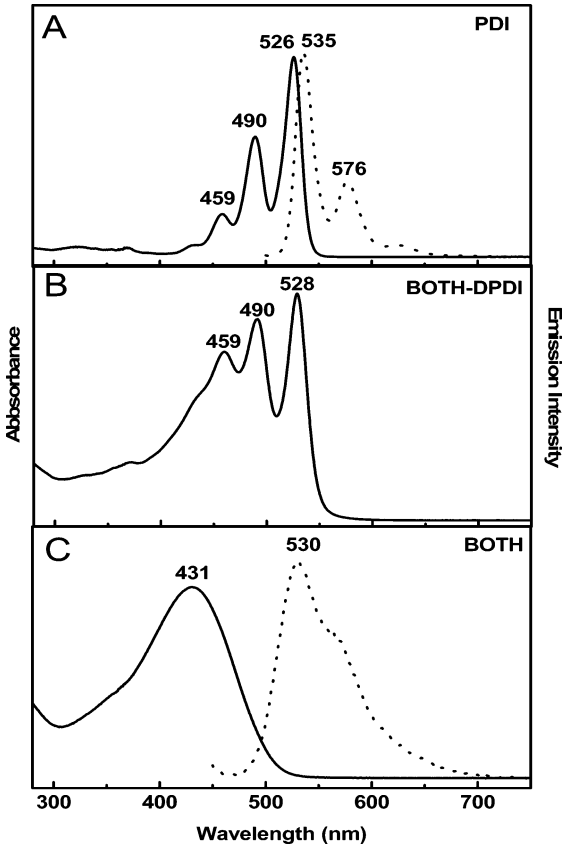

Figure 2. Normalized absorption spectra of (A) **PDI**, (B) **BOTH**−**BPDI**, and (C) **BOTH** in chloroform at room temperature. The dotted lines are, respectively, emission spectra of **PDI** with 490 nm excitation and **BOTH** with 439 nm excitation, both in chloroform at room temperature.

is strong evidence for weak electronic interactions between **PDI** and **BOTH** in the ground-state quartet molecule. In other words, the electron donor and acceptor blocks retain their separate electronic structural entities in the quartet molecule.

Fluorescence spectra of the quartet molecule and the reference compounds **PDI** and **BOTH** were measured in chloroform (Figures 2 and 3). The intense emission band of the reference compound **PDI** ($\lambda_{max} = 535$ nm) shows two vibronic features that are mirror images of its absorption spectrum. Likewise, the strong emission band ($\lambda_{max} = 530$ nm) of the reference compound **BOTH** also has a vibronic splitting. The emission quantum yields for **BOTH** and **PDI** are known to be high at 54% and 97%, respectively.[35,37] However, most of the fluorescence from the **PDI** and **BOTH** blocks is quenched in the quartet molecule when either the **PDI** or **BOTH** block is excited at 490 or 439 nm, respectively. The emission spectrum of the very weak remaining fluorescence of the quartet molecule resembles that of **PDI** rather than **BOTH**, indicating a minor pathway for the energy transfer from the latter to the former. Therefore, the most plausible pathway for >99% of the fluorescence quenching is nonradiative, and likely photoinduced charge separation, which is the focus of this study.

Electrochemical Properties. Electrochemical properties of the quartet molecule were investigated by cyclic voltametry (CV) in methylene chloride at 1 mM concentration using a Pt wire as the working electrode and another Pt wire as the counter electrode. The reduction and oxidation potentials are recorded vs Fc/Fc^+. The same experimental parameters were used to carry out the electrochemical measurements for the reference compounds **PDI** and **BOTH**. The quartet molecule has both

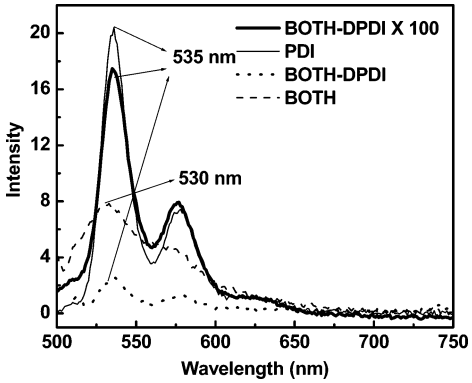

Figure 3. Emission spectra of **PDI** (10^{-8} M in chloroform) and **BOTH**−**DPDI** (10^{-6} M in chloroform) with 439 nm excitation (solid line) and of **BOTH** and **BOTH**−**DPDI** (10^{-8} M in chloroform) with 490 nm excitation (dotted line).

TABLE 1: Half-wave Potentials ($E_{1/2}$ vs Fc/Fc^+) in Methylene Chloride (with 0.1 M n-$Bu_4N^+PF_6^-$) at Room Temperature (CV scan rate 100 mV/s)

	oxidation potentials (V)				reduction potentials (V)	
	PDI	BOTH			PDI	
	$E_{ox(1)}$	$E_{ox(1)}$	$E_{ox(2)}$	$E_{ox(3)}$	$E_{red(1)}$	$E_{red(2)}$
PDI	+1.20				−1.13	−1.37
BOTH		+0.26	+0.61	+1.01		
BOTH−**BPDI**		+0.29	+0.40	+0.61	−1.18	−1.37

reversible oxidative and reductive processes with oxidation potentials (Table 1) at 0.29, 0.40, and 0.61 V, presumably from the **BOTH** block, and reduction potentials at −1.18 and −1.37 V, corresponding to the two reduction steps of the **DPDI** blocks. These electrochemical potentials of the quartet **BOTH**−**BPDI** are indicative of weak electronic interactions between **BPDI** and **BOTH** blocks in the ground state, agreeing with its UV−vis spectra mentioned above.

Molecular Conformations, Frontier Molecular Orbitals, and Energy Levels. The **BOTH**−**BPDI** quartet molecule has two flexible linkages between **PDI** blocks and the benzene ring, which facilitate conformation variations in terms of distances and relative orientations between the donor and acceptor blocks in solution. Hence, there will be an uncertainty in calculating rate constants for the CS and CR processes. To identify the most probable conformations of the quartet molecule in solution, the structural energy minimization using an MM+ force field in vacuo combined with multiple 1-ns trajectory molecular dynamics (MD) simulations were performed using Hyperchem programs (Hypercube). As expected, the **BOTH** backbone of the quartet molecule with two quaterthiophene blocks linked by a benzene ring retains a rigid as well as a nearly planar conformation, while the two **PDI** blocks adopt two very different representative conformations relative to the **BOTH** backbone (Figure 4), one forms $\pi-\pi$ stacking with one of the quarterthiophene blocks and the other forms an extended conformation. Various starting structures were used for the MD simulations, and the resulting structures are similar and well represented in Figure 4. The average center-to-center distances between the **BOTH** and **PDI** blocks are, respectively, ∼11 and ∼14 Å for the $\pi-\pi$ stacked and extended conformations that we refer to from this point on as *proximal* and *distal* conformations, respectively.

The energies and electronic wave function distributions for the frontier molecular orbitals (MOs) clearly demonstrate predominant contributions of the **BOTH** block in the highest occupied molecular orbitals (HOMOs) and those of the **PDI**

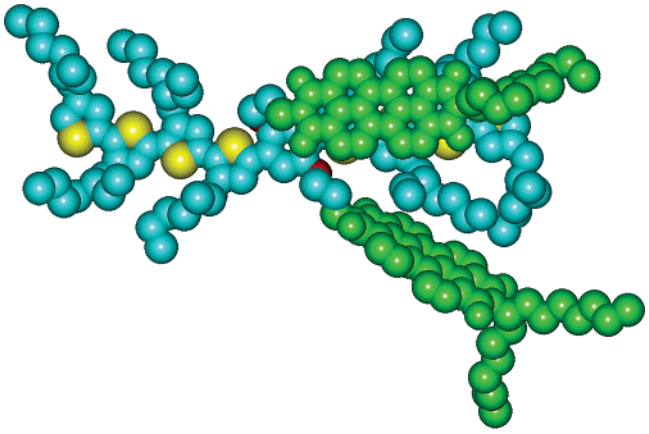

Figure 4. Two representative conformations of the **PDI** blocks (green) relative to the **BOTH** backbone in the quartet molecule calculated from the molecular mechanical energy minimization and molecular dynamics simulations using Hyperchem. The conformation with the average center-to-center distance between **BOTH** and **PDI** blocks of 6−7 Å is referred to as the proximal conformer and that of about 19 Å, the distal conformer.

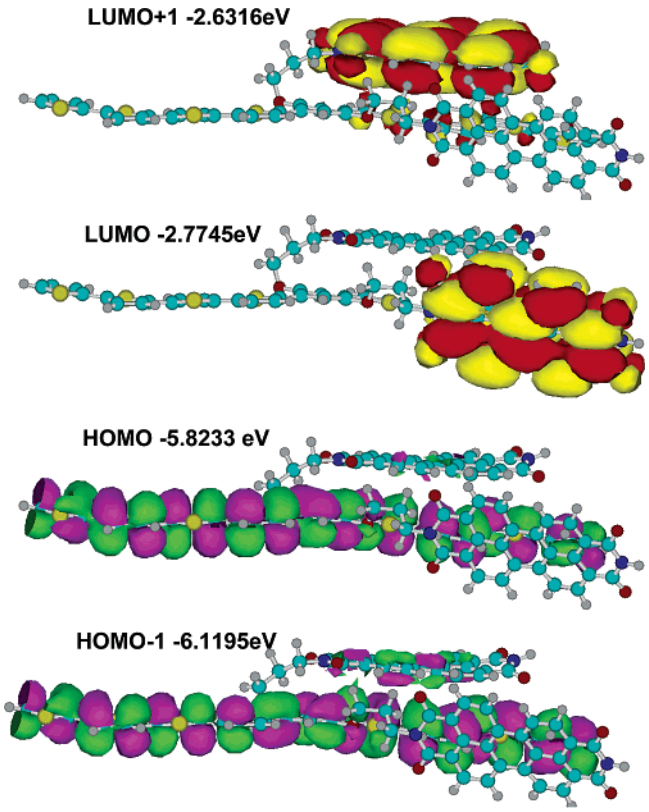

Figure 5. Frontier MOs of the quartet molecule from ZINDO calculations, showing the localization of electron densities of the HOMO on the **BOTH** block and of the LUMO on the **PDI** blocks.

blocks in the lowest unoccupied molecular orbitals (LUMOs) (Figure 5), validating the preferred photoinduced electron-transfer direction from **BOTH** to **PDI** blocks mediated through the lowest energy excited states of the quartet molecule. The MO diagrams also suggest that the entire **BOTH** backbone acts electronically as one entity rather than two separate quatuorthiophene blocks, agreeing with the absorption maximum result mentioned above. Although the two **PDI** blocks have very different orientations relative to the **BOTH** block, the two lowest energy LUMOs have only 0.14 eV difference in energies, while the two highest energy HOMOs differ in energy by nearly 0.3 eV. There is a minor overlap in the wave function distribution

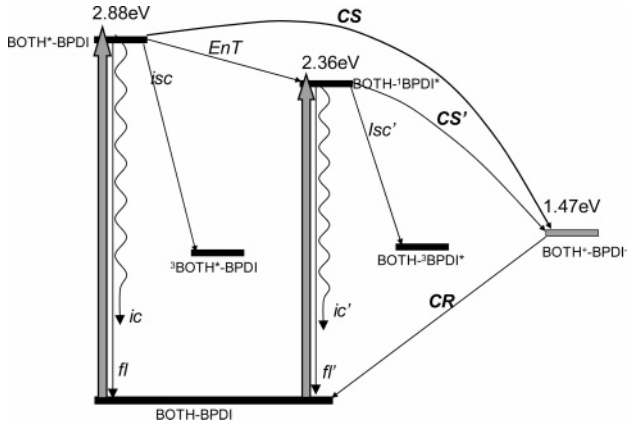

Figure 6. Schematic energy diagram for photophysical processes of the quartet molecule, where CS represents charge separation, EnT, energy transfer, CR, charge recombination, isc, intersystem crossing, ic, internal conversion, and fl, fluorescence.

between the backbone and the **PDI** block in the proximal conformation with the $\pi-\pi$ stacking in a nearly parallel relative orientation.

Photoinduced Electron-Transfer Dynamics. The key processes that determine whether the quartet molecule has the potential as organic photovoltaic material are photoinduced CS and CR. A successful organic photovoltaic material should have a much higher efficiency and rate for CS than for CR. In this report, we mainly focus on the efficiency and dynamics of these processes for molecules in dilute solution while the parallel studies on the solid films with self-assembled molecules and on the prototype devices will follow soon.

According to the electronic spectrum of the quartet molecule and its redox potentials (Table 1), an energy diagram is constructed in Figure 6 for intermediates after the photoexcitation and their respective reaction pathways. The energy gaps between the S_1 state, **BOTH*−BPDI** or **BOTH−BPDI***, and the charge separated state, **BOTH$^+$−PDI$^-$**, are 1.41 and 0.89 eV, respectively, which are sufficiently large and expected to be energetically favorable for the CS process originating from the S_1 state of either the **BOTH*** or **BPDI*** block of the quartet molecule. The latter can be generated via direct photoexcitation or via energy transfer from **BOTH***.

To investigate the kinetics and efficiency of photoinduced CS and CR processes, transient absorption (TA) measurements were carried out for the quartet molecule as well as its reference compounds in toluene and in tetrahydrofuran (THF), respectively. The excitation wavelengths of 403 and 527 nm are used to preferentially excite the **BOTH** and **PDI** blocks, respectively, of the quartet molecule. The **PDI** block has been used as either an electron donor or acceptor in previous studies,[38−41] so that its transient spectral features are well characterized. Unique spectral features in the quartet molecule due to the CS and CR processes can be identified by comparing the TA spectra of the quartet molecule with those of the reference compounds.

The excitation at 403 nm preferentially generates **BOTH*−BPDI** that decays in two possible pathways: (1) energy transfer, **BOTH*−BPDI → BOTH−BPDI***, and (2) electron transfer, **BOTH*−BPDI → BOTH$^+$−BPDI$^-$.** The TA spectra for the quartet molecule as a function of the probe delay time after the excitation (Figure 7) display the time evolution of spectral features corresponding to different intermediates shown in Figure 6. The ground-state bleaching wavelength for the **BOTH** block is beyond the current detection wavelength limit, whereas that for the **BPDI** block is shown as negative TA features around 490 and 530 nm in toluene (485 and 525 nm in THF) as seen

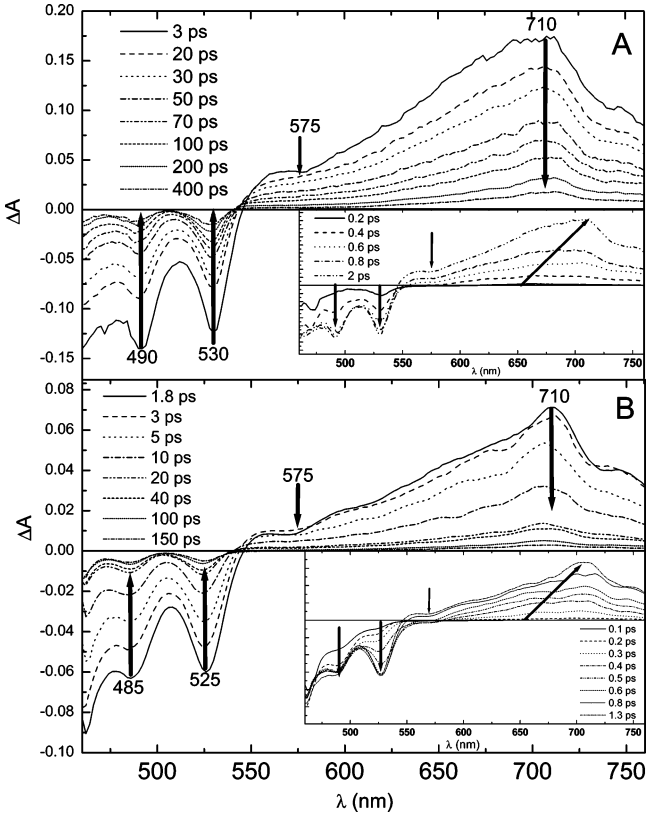

Figure 7. TA spectra of the quartet molecule in toluene (A) and in THF (B).

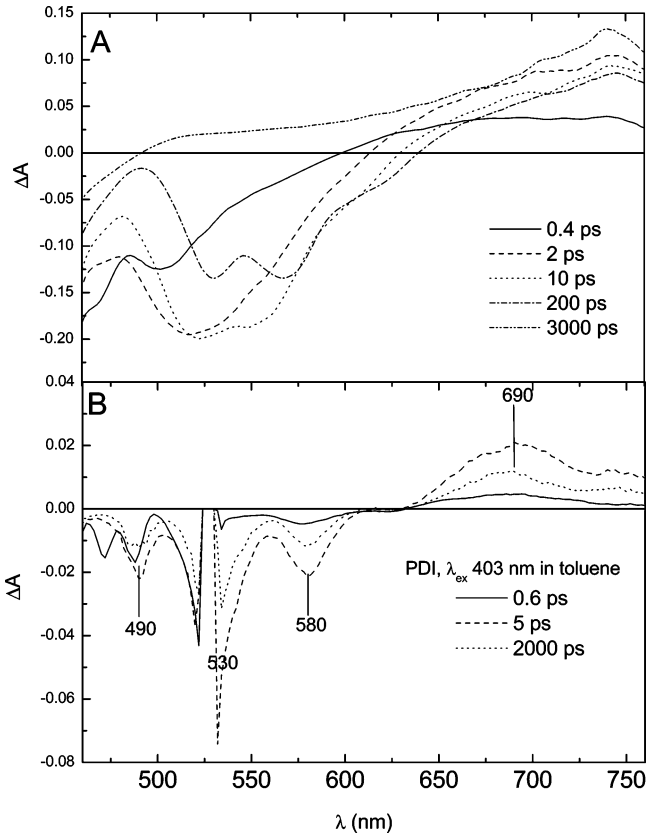

Figure 8. TA of reference compounds **BOTH** (A) and **PDI** (B) in toluene at different delay times after 403-nm excitation.

in Figure 8B. The strong stimulated emission at 525 and 575 nm observed in the reference compound **BOTH** under excitation of the same wavelength (Figure 8A) virtually disappears in the quartet molecule. Meanwhile, the strong stimulated emission shown as a negative peak at 578 nm in the TA spectra of the reference compound **PDI** becomes a barely visible dip in the TA spectra of the quartet molecule immediately after either 403 or 527 nm excitation. Therefore, the main mechanism for the excited state **BOTH***−**BPDI** decay and the fluorescence quenching is associated with the CS process that can proceed via both pathways above. The peak feature around 710 nm is uniquely present in the TA spectra of the quartet molecule, but it is absent in those of the reference compounds. According to previous studies of electrochemistry of the **PDI** block, this feature is mainly due to the formation of the anion $\mathbf{PDI}^-$.[42] The initial TA growth and then decay in the region of 550 to 750 nm and beyond are due to a superimposed absorption from two sources, the excited state **BOTH*** and **PDI*** blocks and the anion $\mathbf{PDI}^-$ generated through the CS process.[42,43] The anion $\mathbf{PDI}^-$ in the quartet molecule is the dominating species, because the excited states **BOTH*** and **PDI*** are rapidly depleted due to the formation of the CS state, $\mathbf{BOTH}^+-\mathbf{BPDI}^-$. The small dip at 575 nm is an indication of the stimulated emission from a very small fraction of the excited state **PDI*** that is only transiently formed via direct excitation at 403 nm or via energy transfer as shown in the first decay pathway. However, the transient **BOTH**−**BPDI*** population is very low according to the TA spectra in Figure 7, and the second pathway dominates, which leads to the CS and CR processes. The rise of the 710-nm feature accompanied by the quenching of the stimulated emission near 575 nm is considered strong evidence for the CS process, and the decay of the 710-nm feature is correlated with the CR process.

TABLE 2: Rate Constants for the Charge Separation and Charge Recombination Reactions of the Quartet Molecule in Different Solvents at 293 K

λ_{ex} (nm)	reaction	A_1 (%)	k_1 (10^{12} s^{-1})	A_2 (%)	k_2 (10^{12} s^{-1})
		Toluene			
403	CS	71	1.47	19	0.149
	CR	72	0.027	18	0.003
527	CS	70	7.14	30	0.326
	CR	75	0.027	25	0.003
		THF			
403	CS	100	2.50		
	CR	86	0.086	14	0.012
527	CS	100	1.30		
	CR	80	0.078	20	0.011

To extract the rate constants for the CS and CR, TA signals detected at 710 nm as a function of the delay time between the pump and probe pulses are fit with multiexponential functions. Table 2 lists the rate constants for the CS and CR processes in toluene and THF. In toluene, dual rate constants are extracted for both CS and CR processes, respectively, with the relative ratio of fast to slow components, 3−4:1. In THF, a single rate constant for the CS process and dual rate constants for the CR process with a fast to slow component ratio of 4:1 are extracted. TA kinetics probed at 686 and 745 nm also fit similar parameters as those at 710 nm due to the broad absorption of anion $\mathbf{PDI}^-$.

The rates for the CS processes are 50−100 times faster than those for the CR processes in both solvents, which make the quartet molecule an excellent candidate for organic photovoltaic material. The rates for the CS processes in THF are faster than in toluene due to the solvation of the CS state by the rapid reorganization through translational and rotational motions of polar THF molecules on the time scale of 0.5 ps[44] that stabilizes the charge separate species. The capability of THF in solvating the charged intermediate equalizes the rates that are otherwise distinctively different, which is in accord with the proximal/

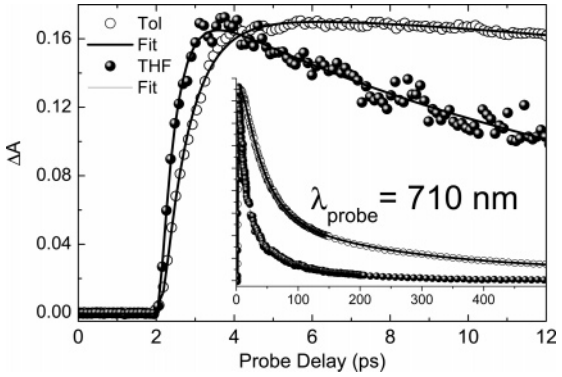

Figure 9. Kinetics curves and their fit functions obtained at a 710-nm probe wavelength with 403-nm excitation.

distal conformation model. The THF solvent reorganization effectively accelerates the slower CS rate of the distal conformation, while it has much less effect on the faster CS rate of the proximal conformation because the donor and acceptor already have very strong interactions due to their wave function overlap as indicated in the ZINDO calculations. The CR process is also sped up in THF compared to toluene, although the driving force for this process is smaller in the former than the latter due to the stabilization energy for the charge separate species. However, the experimental observation of a faster CR process in THF agrees with the energy gap law wherein the nonradiative rate constant increases exponentially with decreasing ground-state−excited-state energy separation.[45] This is an example of interplay between the electronic coupling between the donor and the acceptor with the driving force of the reaction, which is the focus in the discussions below.

To investigate the role of the energy transfer from **BOTH*** to **BPDI** in the quartet molecule, parallel TA measurements were carried out under the excitation at 527 nm which only excites **BPDI** blocks and no energy transfer from **BOTH*** to **BPDI** should be present. However, the dual rate constants are still present for both CS and CR processes in toluene under the excitation at 527 nm. Although the CR rate constants are the same as those under the excitation at 403 nm, the CS rate constants are higher than those obtained with the excitation at 403 nm. This can be explained by excitation wavelength-dependent CS pathways. Under the excitation at 403 nm, there are two parallel pathways leading to the charge separated state **BOTH**$^+$**−BPDI**$^-$, the direct electron transfer **BOTH*−BPDI** → **BOTH**$^+$**−BPDI**$^-$, and the indirect electron transfer **BOTH*−BPDI** → **BOTH−BPDI*** → **BOTH**$^+$**−BPDI**$^-$. However, only one pathway **BOTH−BPDI*** → **BOTH**$^+$**−BPDI**$^-$ is available under the excitation at 527 nm, because **BOTH** has no absorption at 527 nm. Consequently, the CS rate constant with excitation at 527 nm is about 3−5 times that with excitation at 403 nm in toluene and is about twice that in THF. The differences in time responses at the rising edge of the TA kinetic curves (Figure 10) are due to the different reaction pathways as indicated above. The curves in Figure 10 converge after a few picoseconds of excitation, and the CR rate constants are independent of the excitation wavelength, suggesting the same pathways after the initial CS process.

Discussions

The rate and efficiency of photoinduced charge separation are essential factors in photovoltaic applications and intimately related to the structural factors of the donor (D) and the acceptor (A). Several structural parameters, such as relative distances

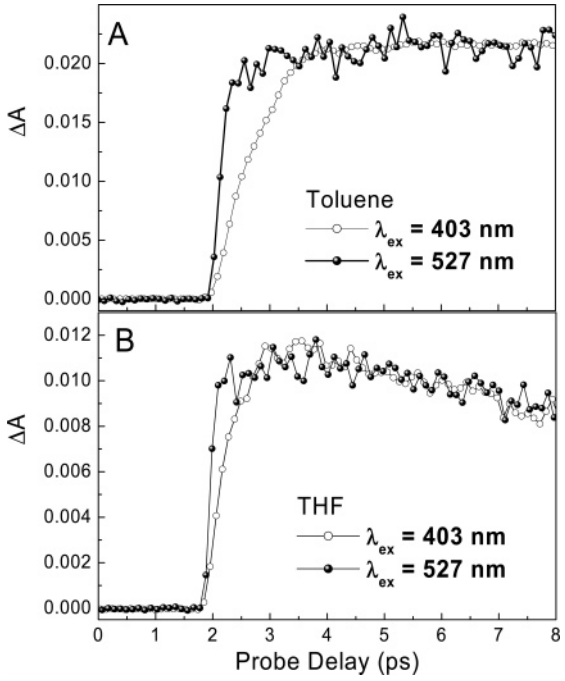

Figure 10. Kinetics traces detected at a 710-nm probe wavelength with different excitation wavelengths as indicated in toluene (A) and in THF (B), showing excitation wavelength-dependent kinetics for the CS process as discussed in the text.

and orientations between D and A, will affect the rate constant of electron-transfer k_{ET}. Because the initial intramolecular charge separation can be considered as a nonadiabatic electron-transfer reaction, its rate constant k_{ET} can be described by the Marcus equation for the electron transfer[46]

$$k_{ET} = \left(\frac{4\pi^2}{h^2 \lambda k_B T}\right)^{1/2} V^2 \exp\left[-\frac{(\Delta G^0 + \lambda)^2}{4\lambda k_B T}\right] \quad (1)$$

where V is the electronic coupling matrix between the donor and the acceptor, ΔG^0 is the free energy of the reaction, and λ is the total reorganization energy and can be expressed as[47]

$$\lambda = \lambda_i + \lambda_s \quad (2)$$

where λ_i and λ_s are the internal and solvent reorganization energies, respectively. If a continuum dielectric constant is used to model the solvent, λ_s can be expressed as[48]

$$\lambda_s = \frac{{e_0}^2}{8\pi\epsilon_0}\left(\frac{1}{2r_D} + \frac{1}{2r_A} - \frac{1}{r_{DA}}\right)\left(\frac{1}{\epsilon_o} - \frac{1}{\epsilon_s}\right) \quad (3)$$

where e_0 is electronic charge and $r_{D,A,DA}$ are radii of the donor and acceptor ions and their center-to-center separation, respectively. ϵ_o and ϵ_s are high frequency and static dielectric constants of the solvent, respectively.

In a polar solvent where the electrochemical potential can be directly measured, the free energy for the CS, ΔG_{CS}, can be approximated by the relationship below[49]

$$\Delta G_{CS} = E_{ox} - E_{red} - E_{0-0} - \frac{{e_0}^2}{\epsilon_s} \quad (4)$$

where E_{0-0} is the energy of the lowest singlet excited state of the donor and E_{ox} and E_{red} are the one electron oxidation and reduction potentials of the donor and acceptor, respectively. As

the solvent polarity decreases, the solvation ability of the solvent for charged ions reduces. The free energies for the CS and CR in any solvent can be expressed by

$$\Delta G_{CS} = E_{ox} - E_{red} - E_{0-0} + \Delta G_d \quad (5)$$

$$\Delta G_{CR} = -E_{ox} + E_{red} - \Delta G_d \quad (6)$$

where ΔG_d is the free energy by which the ion pairs are destabilized and can be written as

$$-\Delta G_d = \frac{e^2}{4\pi\epsilon_0\epsilon_s r_{DA}} + \frac{e^2}{8\pi\epsilon_0}\left(\frac{1}{r_D} + \frac{1}{r_A}\right)\left(\frac{1}{\epsilon_{ref}} - \frac{1}{\epsilon_s}\right) \quad (7)$$

where ϵ_s and ϵ_s' are dielectric constants for the solvent and the reference solvent where the electrochemical potentials are measured.

The dual rate constants of CS and CR processes for the quartet molecule observed in both toluene and THF have two possible origins: (1) the structural diversity of the relative orientations and distances between D and A due to flexible linkages that lead to the proximal and distal conformations and (2) the multiple electron-transfer pathways as mentioned above. The ultrafast TA results favor the first origin, because (a) the dual time constants are still present even only if the **PDI** block is excited by 527 nm light and (b) our recent measurement on a rigidly linked molecule with the same D and A with only one possible r_{DA} gives single rate constants for both the CS and CR processes, respectively (unpublished results). Although the proximal and distal structures of the quartet molecule obtained from the MD simulation likely have their own diverse local structures near the vicinities of the conformations shown in Figure 5, the following discussions on the structure and kinetics correlation will focus on the two averaged structures as an approximation. Hence, the calculations of the parameters for CS and CR below will include the structural parameters extracted from the two representative conformations. While the structure in Figure 5 shows a 1:1 ratio of the distal to the proximal conformation from the MD simulation, the ratio may drastically vary as discussed later.

The 0−0 transition energy E_{0-0} of the **BOTH** donor block is 2.34 eV (530 nm), its one electron oxidation potential $E_{ox} =$ 0.29 eV, and the one electron reduction potential of the **PDI** acceptor block $E_{red} = -1.18$ eV (see Table 1). The r_D and r_A are 5.9 and 4.7 Å assuming **BOTH** is very similar with novithiophene,[50] and the average r_{DA} for the distal and proximal conformations are, respectively, 14.3 and 10.9 Å. ϵ_{ref} (methylene chloride) = 9.1, ϵ_s (toluene) = 2.38, and ϵ_s (THF) = 7.51. According to eqs 5 and 7, ΔG_{CS} for the distal and proximal conformations in toluene are, respectively, −0.44 and −0.57 eV, whereas those corresponding values in THF are, respectively, −0.94 and −0.98 eV. Therefore, there are sufficient free energies for the CS processes in both solvents. The effect of solvent polarity reflected in the dielectric constant is significant for distal conformation, shown by the 0.6 eV difference in ΔG_{CS} that is gained by the solvation of the charge separate state by polar THF. In contrast, the solvent polarity effect is only 0.41 eV for the proximal conformation, whose spacing between the donor and the acceptor may limit the solvent molecule to intervene with the electron transfer. According to the ZINDO (Zerner's Intermediate Neglect of Differential Overlap) calculation conducted in vacuo (Figure 6), molecular orbitals HOMO−1 and LUMO+1 clearly have contributions from the wave functions of **BOTH** and **PDI** in the half of the quartet with the proximal conformation while no wave function overlap is shown in the other half of the quartet molecule with the distal conformation. Therefore, the electronic coupling matrix V for the proximal conformation could be significantly larger than that for the distal conformations, which alone could be a dominating factor responsible for the difference in the rate constants between the two conformations. In addition, values of ΔG_{CS} are qualitatively in accord with the experimentally observed dual CS rate constants of 4×10^{12}/s and 1.7×10^{11}/s in toluene for the proximal and distal conformers, respectively, due to a free energy difference of 0.13 eV, and with the single CS rate constant of 2.5×10^{12}/s in THF, due to a free energy difference of merely 0.04 eV between the two conformations. This assessment also suggests that the fast and slow rates for CS in toluene originate from the structures resembling the proximal and the distal conformation, respectively. The population ratio of the proximal and distal conformations is near 2:1 according to the experimental data, whereas the molecular dynamic simulation suggests a ratio of 1:1. Such a disagreement is likely due to the difference in environments between the experiment in solutions and the simulation in vacuo.

Similarly, the electronic coupling matrix V difference between the two conformations also affects the rate constants for the CR process combined with the effect due to the differences in ΔG_{CR} for the distal and proximal conformations in toluene, −1.90 and −1.77 eV, respectively, and in THF, −1.40 and −1.36 eV, respectively. Hence, the driving force for the CR process is larger in toluene than in THF for distal conformation, which is attributed to the solvation of the charge separated species by THF that lowers the energy of the solvated charge separated state to reduce the energy gap between the charge separated state and the ground state. Despite higher free energies for the CR process in toluene than in THF, the dual reaction rates in the former are, respectively, 2.7×10^{10}/s and 2.8×10^{9}/s, a factor of 3−4 slower than those in the latter, 9.1×10^{10}/s and 1.3×10^{10}/s. Such free energy dependence of the rate constant suggests that the electron transfer for the CR process is in the inverted region of the Marcus equation where the reorganization energy λ is much larger than the free energy of the electron transfer for the charge recombination, ΔG_{CR}.[46] Similar free energy dependence in the CR process has been observed in supermolecules with oligomerphyenylenevinylene (OPV) of different lengths as the electron donor covalently connected with **PDI** blocks as the electron acceptor.[51] The rates for CR are about 100 times slower than the rates for CS, which provides positive prospective for the photovoltaic applications pending on the investigation of the solid-state properties of this material as well as its characteristics in the actual solar cells.

The direct comparison between the reaction rate constants estimated from the multiexponential functions fitting the kinetics data and the calculated rate has proven to be difficult,[47] because the internal reorganization energy λ_i associated with the parameter s in eq 2 is directly derived from the reaction coordination change Δq by a relationship of $\lambda_i = \sum k_j(\Delta q_j)^2/2$, where k_j is the force constant for a particular vibrational mode j. Δq_j is the coordination change from the reactant to the product for a particular vibrational mode j. Since the electron transfer for the CS process takes place between the excited state and the charge separate state of the quartet, and the structure of neither state is available, the internal reorganization energy λ_i could not be calculated directly from the structures. For the same reason of the unknown Δq_j between the charge separate state that acts as the reactant and the ground state as the product for the electron transfer in the CR process, the internal reorganization energy would not be available either from the structures.

TABLE 3: Energetic and Kinetic Parameters of Electron-Transfer Processes

process	solvent	conformation	$\Delta G°$ (eV)	λ_s (eV)
CS	toluene	distal	−0.50	0.02
		proximal	−0.79	0.01
	THF	distal	−0.96	0.30
		proximal	−1.05	0.17
CR	toluene	distal	−1.84	0.02
		proximal	−1.55	0.01
	THF	distal	−1.38	0.30
		proximal	−1.29	0.17

However, the well-known Marcus equation for chemical reaction dynamics describes the correlation between the activation energy $\Delta G^{\ddagger}$, the free energy $\Delta G°$, and the reorganization energy λ as shown below

$$\Delta G^{\ddagger} = \frac{(\Delta G^0 + \lambda)^2}{4\lambda} \tag{8}$$

which is based on assumptions of quadratic potential surfaces with the same curvature for all the states involved in the reactions.[48] In this study, only the solvent reorganization energy λ_s for each process is calculated and tabulated with the free energy and rate constants in Table 3. Although the small λ_s in toluene is expected for a nonpolar solvent, the λ_s in THF is significantly lower than other donor−acceptor supermolecules studied previously.[49] This may be a sign of over approximation in applying the Marcus equation to the long and conjugated **BOTH** block. A precise calculation would take the actual charge density distribution of different blocks as well as the analytical expression on the r_{DA} distribution which is beyond the scope of this paper.

Conclusion

A new donor/acceptor quartet molecule with bis-oligothiophene (**BOTH**) and bis-perylenediimide (**BPDI**) blocks attached to a benzene ring was synthesized. The electronic structures and dynamics of photoinduced charge separation of this compound and the reference compounds were characterized in dilute solution. It was found that this molecular system exhibits a more efficient charge separation than charge recombination processes in both polar and nonpolar organic solvents. The results strongly suggest that both through-bond and through-space electron-transfer processes exist, as evidenced by the two different dynamics of charge separation and recombination associated with two types of donor/acceptor pair conformations in solution. The results also imply that the short flexible spacers between donors and acceptors provide enough flexibility for reorganization of the moieties, yet small enough barriers for charge separation. This study provides initial results for further investigation of its organic photovoltaic applications, which involve the next level of molecular self-assembly into films and prototype devices.

Acknowledgment. This work is supported by the Division of Chemical Sciences, Office of Basic Energy Sciences, the U. S. Department of Energy under Contract W-31-109-Eng-38 (for L.X.C.). We gratefully acknowledge the financial supports of the National Science Foundation and the NSF MRSEC program at The University of Chicago and AFOSR. UC-Argonne Nanoscience Consortium (L.Y. and S.X.) and UC/ANL collaborative seed grant (L.Y. and L.X.C.) provided partial support of this research. We thank Dr. Dmitrii Polshakov for helpful discussions.

Supporting Information Available: General synthesis and schematic representations of the compounds presented along with a table displaying characteristics of each. This material is available free of charge via the Internet at http://pubs.acs.org.

References and Notes

(1) Blankenship, R. E. *Molecular Mechanisms of Photosynthesis*; Balckwell Science: Oxford, U.K., 2002.

(2) Fromme, P.; Kern, J.; Loll, B.; Biesiadka, J.; Saenger, W.; Witt, H. T.; Krauss, N.; Zouni, A. *Philos. Trans. R. Soc. London, Ser. B* **2002**, *357*, 1337.

(3) Brixner, T.; Stenger, J.; Vaswani, H. M.; Cho, M.; Blankenship, R. E.; Fleming, G. R. *Nature* **2005**, *434*, 625.

(4) Boxer, S. G.; Lockhart, D. J.; Kirmaier, C.; Holten, D. *Jerusalem Symp. Quantum Chem. Biochem.* **1990**, *22*, 39.

(5) Chan, C. K.; DiMagno, T. J.; Chen, L. X. Q.; Norris, J. R.; Fleming, G. R. *Proc. Natl. Acad. Sci. U.S.A.* **1991**, *88*, 11202.

(6) Heller, B. A.; Holten, D.; Kirmaier, C. *Science* **1995**, *269*, 940.

(7) Jortner, J.; Bixon, M. *Electron transfer in bacterial photosynthesis*; 1986; Vol. 3.

(8) Moser, C. C.; Page, C. C.; Dutton, P. L. Photosynthesis: Bacterial Reaction Center. In *Electron Transfer in Chemistry*; Balzani, V., Ed.; Wiley-VCH: Weinheim, Germany, 2001; Vol. 3, p 24.

(9) Pettersson, K.; Kilsa, K.; Martensson, J.; Albinsson, B. *J. Am. Chem. Soc.* **2004**, *126*, 6710.

(10) Wasielewski, M. R. *Chem. Rev.* **1992**, *92*, 435.

(11) Lukas, A. S.; Bushard, P. J.; Weiss, E. A.; Wasielewski, M. R. *J. Am. Chem. Soc.* **2003**, *125*, 3921.

(12) Guldi, D. M.; Luo, C. P.; Prato, M.; Troisi, A.; Zerbetto, F.; Scheloske, M.; Dietel, E.; Bauer, W.; Hirsch, A. *J. Am. Chem. Soc.* **2001**, *123*, 9166.

(13) Lewis, F. D.; Wu, T. F.; Liu, X. Y.; Letsinger, R. L.; Greenfield, S. R.; Miller, S. E.; Wasielewski, M. R. *J. Am. Chem. Soc.* **2000**, *122*, 2889.

(14) Chen, L. X.; Lee, P. L.; Gosztola, D.; Svec, W. A.; Wasielewski, M. R. *J. Synchrotron Radiat.* **1999**, *6*, 403.

(15) Kuciauskas, D.; Liddell, P. A.; Lin, S.; Johnson, T. E.; Weghorn, S. J.; Lindsey, J. S.; Moore, A. L.; Moore, T. A.; Gust, D. *J. Am. Chem. Soc.* **1999**, *121*, 8604.

(16) Peumans, P.; Forrest, S. R. *Appl. Phys. Lett.* **2001**, *79*, 126.

(17) Xue, J. G.; Uchida, S.; Rand, B. P.; Forrest, S. R. *Appl. Phys. Lett.* **2004**, *85*, 5757.

(18) Loi, M. A.; Denk, P.; Hoppe, H.; Neugebauer, H.; Winder, C.; Meissner, D.; Brabec, C.; Sariciftci, N. S.; Gouloumis, A.; Vazquez, P.; Torres, T. *J. Mater. Chem.* **2003**, *13*, 700.

(19) Peumans, P.; Forrest, S. R. *Appl. Phys. Lett.* 2002, *80*, 338.

(20) Stubinger, T.; Brutting, W. *J. Appl. Phys.* **2001**, *90*, 3632.

(21) Kerp, H. R.; Donker, H.; Koehorst, R. B. M.; Schaafsma, T. J.; van Faassen, E. E. *Chem. Phys. Lett.* **1998**, *298*, 302.

(22) Gregg, B. A. *J. Phys. Chem.* **1996**, *100*, 852.

(23) Wohrle, D.; Kreienhoop, L.; Schlettwein, D. *Phthalocyanines* **1996**, *4*, 219.

(24) Liu, J. S.; Tanaka, T.; Sivula, K.; Alivisatos, A. P.; Frechet, J. M. J. *J. Am. Chem. Soc.* **2004**, *126*, 6550.

(25) Fogg, D. E.; Radzilowski, L. H.; Dabbousi, B. O.; Schrock, R. R.; Thomas, E. L.; Bawendi, M. G. *Macromolecules* **1997**, *30*, 8433.

(26) Neuteboom, E. E.; Meskers, S. C. J.; van Hal, P. A.; van Duren, J. K. J.; Meijer, E. W.; Janssen, R. A. J.; Dupin, H.; Pourtois, G.; Cornil, J.; Lazzaroni, R.; Bredas, J. L.; Beljonne, D. *J. Am. Chem. Soc.* **2003**, *125*, 8625.

(27) de Boer, B.; Stalmach, U.; van Hutten, P. F.; Melzer, C.; Krasnikov, V. V.; Hadziioannou, G. *Polymer* **2001**, *42*, 9097.

(28) Haugeneder, A.; Neges, M.; Kallinger, C.; Spirkl, W.; Lemmer, U.; Feldmann, J.; Scherf, U.; Harth, E.; Gugel, A.; Mullen, K. *Phys. Rev. B* **1999**, *59*, 15346.

(29) Markov, D. E.; Amsterdam, E.; Blom, P. W. M.; Sieval, A. B.; Hummelen, J. C. *J. Phys. Chem. A* **2005**, *109*, 5266.

(30) Peumans, P.; Uchida, S.; Forrest, S. R. *Nature* **2003**, *425*, 158.

(31) Yang, X. N.; Loos, J.; Veenstra, S. C.; Verhees, W. J. H.; Wienk, M. M.; Kroon, J. M.; Michels, M. A. J.; Janssen, R. A. J. *Nano Lett.* **2005**, *5*, 579.

(32) van Duren, J. K. J.; Loos, J.; Morrissey, F.; Leewis, C. M.; Kivits, K. P. H.; van Ijzendoorn, L. J.; Rispens, M. T.; Hummelen, J. C.; Janssen, R. A. J. *Adv. Func. Mater.* **2002**, *12*, 665.

(33) Hasharoni, K.; Levanon, H.; Greenfield, S. R.; Gosztola, D. J.; Svec, W. A.; Wasielewski, M. R. *J. Am. Chem. Soc.* **1996**, *118*, 10228.

(34) Greenfield, S. R.; Wasielewski, M. R. *Opt. Lett.* **1995**, *20*, 1394.

(35) Grebner, D.; Helbig, M.; Rentsch, S. *J. Phys. Chem.* **1995**, *99*, 16991.

(36) Chen, L. X.; Jaeger, W. J. H.; Niemczyk, M. P.; Wasielewski, M. R. *J. Phys. Chem. A* **1999**, *103*, 4341.

(37) Du, H.; Fuh, R. C. A.; Li, J. Z.; Corkan, L. A.; Lindsey, J. S. *Photochem. Photobiol.* **1998**, *68*, 141.

(38) van der Boom, T.; Hayes, R. T.; Zhao, Y. Y.; Bushard, P. J.; Weiss, E. A.; Wasielewski, M. R. *J. Am. Chem. Soc.* **2002**, *124*, 9582.

(39) Lukas, A. S.; Zhao, Y. Y.; Miller, S. E.; Wasielewski, M. R. *J. Phys. Chem. B* **2002**, *106*, 1299.

(40) Wurthner, F.; Chen, Z. J.; Hoeben, F. J. M.; Osswald, P.; You, C. C.; Jonkheijm, P.; von Herrikhuyzen, J.; Schenning, A.; van der Schoot, P.; Meijer, E. W.; Beckers, E. H. A.; Meskers, S. C. J.; Janssen, R. A. J. *J. Am. Chem. Soc.* **2004**, *126*, 10611.

(41) Ramos, A. M.; Beckers, E. H. A.; Offermans, T.; Meskers, S. C. J.; Janssen, R. A. J. *J. Phys. Chem. A* **2004**, *108*, 8201.

(42) Gosztola, D.; Niemczyk, M. P.; Svec, W.; Lukas, A. S.; Wasielewski, M. R. *J. Phys. Chem. A* **2000**, *104*, 6545.

(43) Angadi, M.; Gosztola, D.; Wasielewski, M. R. *Mater. Sci. Eng. B,* **1999**, *63*, 191.

(44) Bedard-Hearn, M. J.; Larsen, R. E.; Schwartz, B. J. *J. Phys. Chem. B* **2003**, *107*, 14464.

(45) Freed, K. F.; Jortner, J. *J. Chem. Phys*. **1970**, *52*, 6272.

(46) Marcus, R. A. *J. Chem. Phys.* **1965**, *43*, 3477.

(47) Barbara, P. F.; Meyer, T. J.; Ratner, M. A. *J. Phys. Chem.* **1996**, *100*, 13148.

(48) Overing, H.; Paddon-Row, M. N.; Heppener, M.; Oliver, A. M.; Cotsaris, E.; Verhoeven, J. W.; Hush, N. S. *J. Am. Chem. Soc.* **1987**, *109*, 3258.

(49) Sakata, Y.; Tsue, H.; Oneil, M. P.; Wiederrecht, G. P.; Wasielewski, M. R. *J. Am. Chem. Soc.* **1994**, *116*, 6904.

(50) Ramos, A. M.; Meskers, S. C. J.; van Hal, P. A.; Knol, J.; Hummelen, J. C.; Janssen, R. A. J. *J. Phys. Chem. A* **2003**, *107*, 9269.

(51) Davis, W. B.; Svec, W. A.; Ratner, M. A.; Wasielewski, M. R. *Nature* **1998**, *396*, 60.